Appl. Phys. A 80, 1257–1263 (2005)
DOI: 10.1007/s00339-004-3157-1

Applied Physics A
Materials Science & Processing

Z. LI[1,✉]
B. RAJENDRAN[1]
T.I. KAMINS[1]
X. LI[1]
Y. CHEN[2]
R. STANLEY WILLIAMS[1]

Silicon nanowires for sequence-specific DNA sensing: device fabrication and simulation

[1] Quantum Science Research, Hewlett-Packard Laboratories, 1501 Page Mill Road, MS 1123, Palo Alto, CA 94304, USA
[2] University of California, Los Angeles, School of Engineering and Applied Science, 48-121 Engr. IV Bldg, Box 951597, Los Angeles, CA 90095-1597, USA

Received: 14 September 2004/Accepted: 23 November 2004
Published online: 11 March 2005 •

ABSTRACT Highly sensitive, sequence-specific and label-free DNA sensors were demonstrated by monitoring the electronic conductance of silicon nanowires (SiNWs) with chemically bonded single-stranded (ss) DNA or peptide nucleic acid (PNA) probe molecules. For a 12-mer oligonucleotide, tens of pM of target ss-DNA in solution was recognized when the complementary DNA oligonucleotide probe was attached to the SiNW surfaces. In contrast, ss-DNA samples of $\times 1000$ concentration with a single-base mismatch produce only a weak signal due to nonspecific binding. In order to gain a physical understanding of the change in conductance of the SiNWs with the attachment of the DNA targets and the probes, process and device simulations of the two-dimensional cross sections of the SiNWs were performed. The simulations explained the width dependence of the SiNW conductance and provided understanding to improve the sensor performance.

PACS 85.35.-p; 87.83.+a; 07.07.Df

1 Introduction

One-dimensional nanostructures have been demonstrated as good candidates for ultra-sensitive, miniaturized molecule sensors [1]. A wide variety of systems have been explored. Sensors based on semiconductor nanostructures, such as semiconductor single-wall carbon nanotubes [2–4], silicon nanowires (SiNWs) [5–7], SnO_2 nanowires [8], and In_2O_3 nanowires [9] can be generally understood in terms of the change of mobile charge, and hence the conductivity, of the nanostructures by the presence or absence of molecular species. Currently, most of the existing studies based on 'bottom-up' nanostructures are limited by complex integration, requiring transfer and positioning of individual nanostructures and by the difficulty of making reliable ohmic contacts. Furthermore, the control of doping concentrations in self-assembled semiconducting nanostructures remains a challenge, and the fabrication of high-density sensor arrays is also very difficult. As reported previously [6], we have developed a process to fabricate silicon nanowire sensors based on 'top-down' semiconductor processing. After chemically immobilizing single-stranded (ss) DNA probes on the surfaces of such silicon nanowires, target DNA solutions of a few tens of pM concentration were recognized, with the capability of discriminating against single-base mismatch in the DNA sequence. In this paper, further experimental work and device simulations of the two-dimensional (2D) cross sections of the SiNWs are reported. This combination provides a physical understanding of the change in conductance of the SiNWs as the DNA targets and probes are attached. In particular, an understanding of the width dependence of the SiNW conductance and means for improving the sensor performance are provided by the results of numerical simulation.

✉ Fax: +1-650-236-9885, E-mail: zhiyong.li@hp.com

2 Experimental method

2.1 Si *nanowire fabrication procedure*

Si-based nanoscale sensors were fabricated using silicon-on-insulator (SOI) wafers (Soitec, France). The SOI wafers, which initially had a 100-nm single-crystal silicon layer on a 200-nm-thick SiO_2 insulating layer, were first thermally oxidized to reduce the silicon-layer thickness to 50 nm. The 115-nm-thick, thermally grown silicon dioxide on the top was then thinned to 50 nm by HF etching to allow the subsequent doping process. The wafers were doped by ion implanting with boron or phosphorus to produce concentrations between 10^{16} /cm^3 and 10^{19} /cm^3; implantation was followed by heating at 1025 °C in a N_2 ambient for 20 s. The silicon layer was protected with the 50-nm thermal oxide to prevent dopant loss during the high-temperature activation, and the activation procedure used in this study was also carefully selected to generate a uniform dopant distribution in the silicon layer. The top silicon layer was then patterned by electron-beam lithography (for nanowires) and optical lithography (for micron-scale electrical leads). The patterns of the SiNWs and their micron-scale electrical leads were transferred to the upper silicon layer by reactive ion etching (RIE). The micron-scale electrical leads were subjected to another ion implantation with the same doping type as the SiNWs, but with a concentration of $> 10^{20}$ /cm^3. The remaining thermal oxide on top of the silicon layer was completely removed by HF etching after the contact-implantation step. To decrease the density of surface dangling bonds on the Si surface and increase the stability of the sensors, a high-quality SiO_2 layer with a thickness of 3 nm was grown on the Si nanowire surfaces

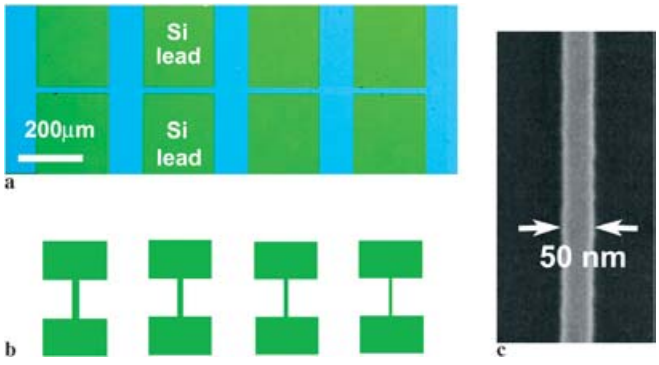

FIGURE 1 (**a**) Optical image of the central region of a sensor test chip showing a portion of the lead and the bridged nanowire (barely visible under the optical microscope) used for the DNA sensing study; (**b**) schematic drawing of the SiNWs with varying widths corresponding to the image in (**a**); (**c**) a representative SEM image showing a portion of a 50-nm-wide SiNW, which extends between two contact leads

at 925 °C in an O_2 ambient for 1 min. A 100-nm-thick aluminum layer was deposited by electron-beam evaporation on top of the silicon contact regions after preferentially removing the 3-nm SiO_2 layer (using 1:10 HF solution) from these areas to allow electrical contact with the Si and reduce the resistance of the electrical leads. The samples were then annealed in forming gas (3.8% hydrogen in nitrogen) at 450 °C for 30 min to make reliable ohmic contact between the Al and the Si, as well as to passivate the interface states between the SiNWs and the thermal oxide. SiNWs with widths of 50 nm, 100 nm, 200 nm, 400 nm, and 800 nm were fabricated to study the size dependence, as discussed in later sections. The final thickness of the silicon layer was 50 nm. Figure 1 shows a typical optical micrograph of the central region of a sensor chip and a scanning electron microscope (SEM) image of a 50-nm-wide SiNW.

2.2 Si *nanowire functionalization procedure*

After the fabrication of the SiNWs and the electrical leads, the devices were chemically functionalized with probe molecules for DNA sensing experiments. Previously reported methods based on covalent binding [10–12] were adopted to immobilize single-stranded DNA or peptide nucleotide acid (PNA) probes on the SiNWs. Compared with noncovalent attachment methods [13], the covalent anchoring of oligonucleotides on the SiNW surface can provide better stability and less nonspecific hybridization for DNA sensing. The functionalization procedure is schematically shown in Fig. 2 for PNA probe attachment. Before attaching the probe, the surfaces of the SiNWs were treated with a water-vapor plasma. The plasma treatment (1) cleaned the sample surfaces and (2) generated more hydrophilic surfaces by hydroxy terminating the silicon-oxide surfaces. A self-assembled monolayer with terminal thiols was then prepared by exposing the surface to the vapor of 3-mercaptopropyltrimethoxysilane (MPTMS, Aldrich, Milwaukee, WI) in argon for 4 h [14], followed by rinsing with absolute ethyl alcohol and blowing dry with nitrogen. For the PNA probe attachment, a similar procedure as that for the DNA probe attachment [6] was used. The PNA probe molecule was custom synthesized with an acrylic amidite terminal group (Biosynthesis

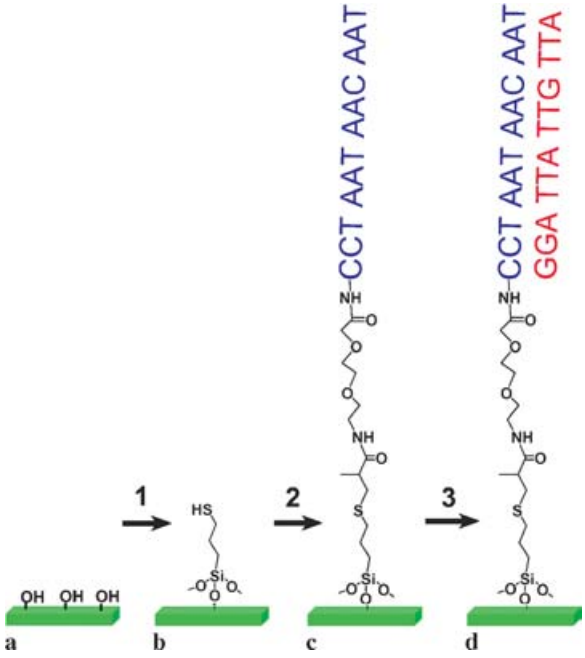

FIGURE 2 The modification scheme of the SiNW surface with PNA probe for the DNA sensor: (1) self-assembly of 3-mercaptopropyltrimethoxysilane (MPTMS) by gas-phase reaction in Ar for 4 h; (2) covalent immobilization of PNA probes by exposing the previous surface to 5 μM solution of oligonucleotide CCT AAT AAC AAT modified with acrylic amidite at the N-terminal for 12 h; (3) DNA detection based on hybridization between label-free complementary DNA target GGA TTA TTG TTA and the immobilized PNA probes on the SiNW surfaces. The orientation of oligonucleotide molecules on the surface is drawn normal to the surface only for illustration

Inc., Lewisville, TX). The SiNW surfaces were exposed to a 5 μM PNA solution in water for 12 h. The sensor devices were rinsed with deionized (DI) water and blown dry with nitrogen. A series of control samples, which were used for surface characterization, were made on unpatterned oxidized silicon wafers following the same functionalization procedure as for the nanowire sensor devices. The immobilization of DNA or PNA probes was confirmed by surface photo-voltage (SPV) measurements [15], X-ray photoelectron spectrometry (XPS), and time-of-flight secondary-ion mass spectrometry (TOF-SIMS).

2.3 *Device test procedure*

The electrical measurements were performed using a Keithley 4200 semiconductor parameter analyzer (Keithley Instruments Inc., Cleveland, OH). Before functionalizing the SiNWs, dry testing of the fabricated nanowires was performed to measure the current–voltage (I–V) properties of nanowires with varying widths. For the functionalized SiNWs, sequence-specific DNA detection was achieved by monitoring the conductance of the SiNWs while the target DNA solution was injected into a purpose-built testing apparatus for the sensor chips. Only high-purity water ($> 18\,\mathrm{M}\Omega$, Nanopure, Barnstead, IA) was used as the solvent in this study, since charge-based detection is most sensitive when counter-ion screening of the negatively charged DNA molecules is minimized. In this case, most of the counter ions are already bound to the charged probe or target molecules.

3 Results and discussion

3.1 SiNWs *dry electrical test*

The quality of as-fabricated SiNWs was characterized electrically in air by measuring two-terminal current–voltage characteristics. Typically, the I–V characteristics of the SiNWs were linear, and the conductance generally scaled proportionally with the dimension of the SiNWs, as shown by the triangular data points in Fig. 3, indicating that good ohmic contact between the contact pads and the SiNWs was formed. However, we did observe some scatter in the data for the 50-nm-wide SiNWs and significant nonproportional scaling of the conductance for this width, as will be discussed later.

3.2 *Surface characterization*

The direct characterization of the attachment of oligonucleotide probes onto small SiNWs is extremely difficult with existing technologies; therefore, we used unpatterned silicon wafers to follow the functionalization steps of the SiNW sensors. Both X-ray photoelectron spectrometry (XPS) and time-of-flight secondary-ion mass spectrometry (TOF-SIMS) were used in this study to characterize the PNA immobilization. A representative regional spectrum for the PNA-functionalized surface is shown in Fig. 4a, curve (i). For comparison, the XPS spectrum of the sample prior to PNA attachment is shown in Fig. 4a, curve (ii). As indicated from the two spectra, the N 1*s* peak is observed on the PNA-functionalized surface, whereas it did not exist on the sample prior to PNA attachment; a significant increase of intensity was also observed for the C 1*s* peak. Both observations indicate the successful immobilization of the PNA molecules on the surface. The same samples were also characterized by TOF-SIMS. As shown in the positive-mode TOF-SIMS spectra in Fig. 4b, peaks corresponding to fragments of the nucleotides adenine (molecular weight 136), cytosine (molecular weight 112), and thymine (molecular weight 129) were detected; these species are associated with the PNA probes (CCT AAT AAC AAT) on the surface. However, one unexpected peak at position 152, which is the molecular weight of guanine, was also observed in the TOF-SIMS spectra of PNA-functionalized surfaces. However, there are no guanine units in the sequence of the PNA probe studied. By examining the backbone of the PNA, we concluded that the peak at 152 is due to a fragment from the backbone of the PNA molecule with the chemical formula of $C_7H_8N_2O_2$, instead of guanine.

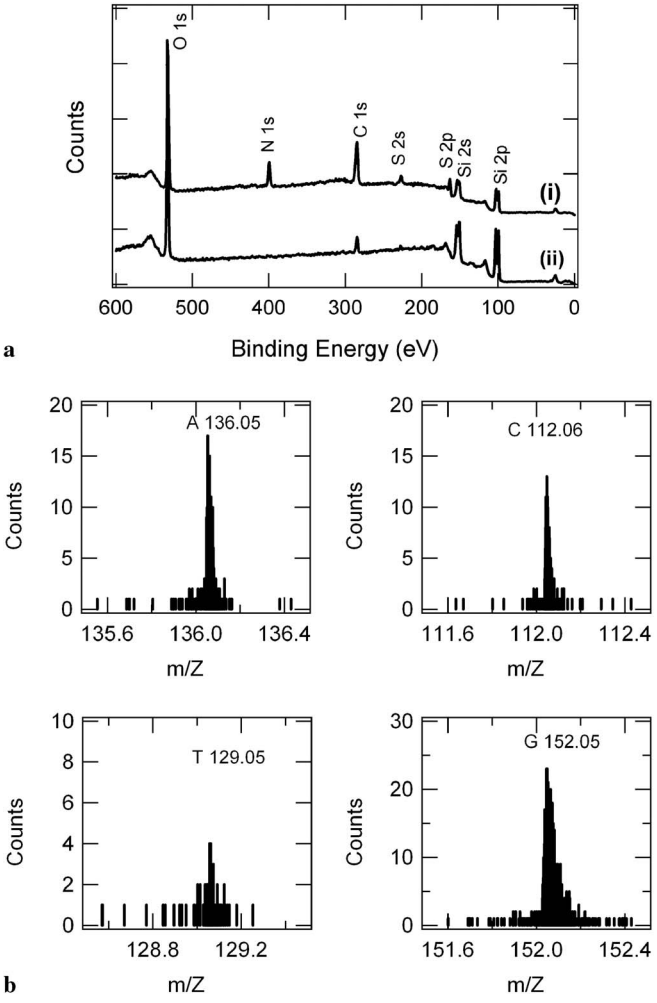

FIGURE 4 (**a**) XPS survey spectra of (i) PNA probe (CCT AAT AAC AAT) functionalized surface and (ii) the surface prior to the PNA attachment; (**b**) TOF-SIMS spectra of the PNA probe functionalized surface; selected mass regions in positive-ion detection mode

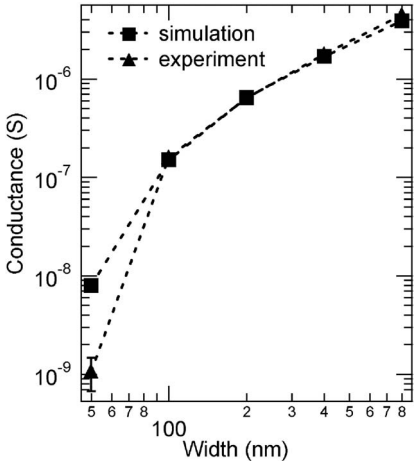

FIGURE 3 Comparison between the simulated and experimental values of the conductance as a function of wire width. The charge density at the oxide–semiconductor interface is assumed to be 1×10^{12} /cm^2

3.3 *Device* DNA *sensing test*

According to Wang et al. [16], PNA probes offer significant advantages for sequence-specific DNA sensing compared to DNA probes, including higher sensitivity and specificity, faster hybridization at room temperature, and minimal dependence on ionic strength of the solution. Since we have reported in detail on DNA-functionalized nanowire sensors previously, we focus on PNA-functionalized nanowire sensors here. Figure 5 shows the real-time response of five different sensors with various widths when exposed to DNA solutions. The five sensors were p-type, boron-doped (nominal 10^{19} /cm^3) wires with physical dimensions of 20-μm length and 50-nm thickness and were functionalized with probes

of the sequence 5'-CCT AAT AAC AAT-3', as described in Sect. 2. Before the exposure of the sensor surfaces to any DNA solution, deionized water was flowing over the sensors to initialize the sensor test, as shown in region I in Fig. 5. Since there is no analyte in pure water, the conductance of the sensor wires did not change with time. In region II, 200 μL of the noncomplementary DNA (3'-GGA TCA TTG TTA-5') solution with 10 nM concentration was injected over the sensor surface. A small signal increase was detected, which was attributed to nonspecific DNA binding events on the sensor surfaces. In region III, 200 μL of the complementary DNA (3'-GGA TTA TTG TTA-5') solution with a concentration of 10 pM was injected over the sensor surface. No water rinsing was performed between injections. After a transition associated with the injection procedure, a significant steady-state conductance increase was observed for all the sensors. The increase of the signal resulted from the specific binding of the target DNA with the probes on the surfaces of the nanowires. Further injection of a higher concentration of the target DNA solution (100 pM), as shown in region IV, only increased the conductance slightly. Since the majority of the probes on the sensor surfaces were hybridized with the target DNA molecules in region III, few unoccupied binding sites were available for the additional molecules introduced into the solution.

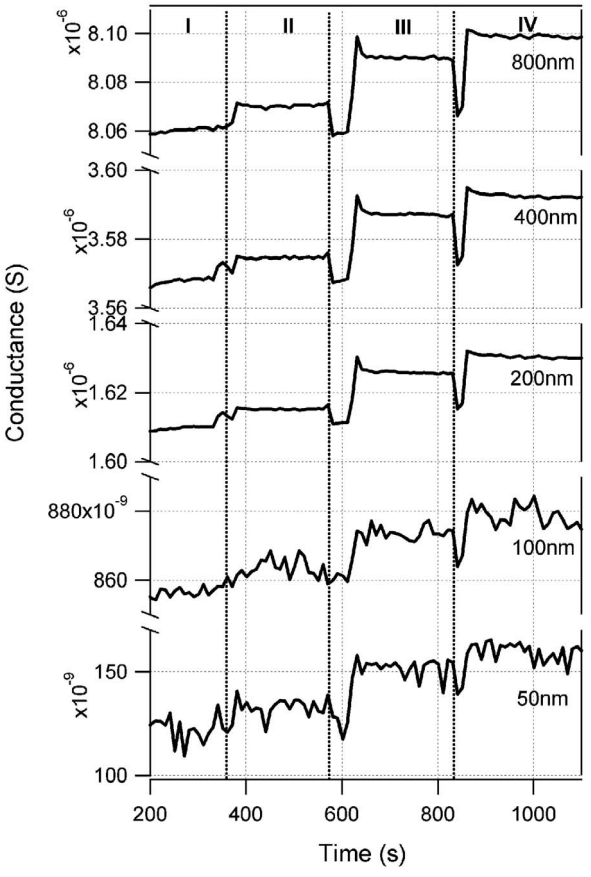

FIGURE 5 Time response of DNA detection on five sensors with different nanowire widths at four stages of the experiment. I: DI water; II: 10 nM noncomplementary DNA solution; III: 10 pM complementary DNA solution; and IV: 100 pM complementary DNA solution

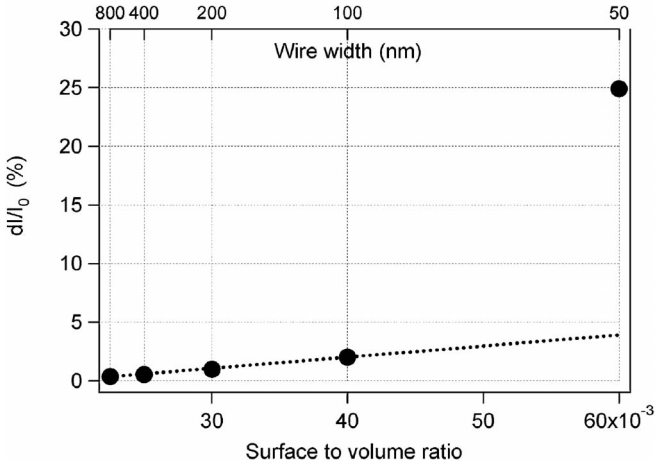

FIGURE 6 The relationship between sensitivity for DNA detection and the surface-to-volume ratio of the nanowires. The *dotted line* represents the linear trend based on the experimental data for 800–100 nm wires

Comparing our PNA-functionalized SiNWs with our previously reported DNA-functionalized SiNWs [6] for the same doping type (p-type with 10^{19} /cm^3) and dimension (50-nm wide), the PNA-functionalized device showed a 25% response at 10 pM DNA solution, whereas the DNA-functionalized device showed a 12% response at 25 pM DNA solution (response is defined as $(I_{\mathrm{DNA}} - I_0)/I_0$). Therefore, the PNA-functionalized SiNW was about four times as sensitive as the DNA-functionalized one (defining sensitivity as response/concentration). The improved sensitivity of the PNA probe is consistent with the observations of Wang et al. [16]. However, even with the improved performance of the PNA probes on our SiNW sensors, we were not able to detect 100 fM concentrations of DNA as reported by Hahm and Lieber [7]. This discrepancy deserves further investigation, especially with regard to the details of the sample geometry and test protocol.

The response of the sensors was further analyzed by plotting the sensitivity (defined as the ratio of conductance change to the baseline conductance in region I) as a function of the surface-to-volume ratio of the sensors (defined in terms of the nanowire dimensions as (2 × height + width)/(width × height)). The result is shown in Fig. 6. For wires with widths in the range of 800 nm to 100 nm, the sensitivity varied linearly with the width. For the 50-nm-wide sensor, the experimentally observed sensitivity (filled circle) was much greater than the value extrapolated from the linear fit (dashed line in Fig. 6). The large enhancement of sensitivity for the 50-nm nanosensor suggests that, as we miniaturize the sensor to even smaller dimensions, we may achieve nanosensors with much higher sensitivity and even lower detection limits for DNA molecules. Consequently, further investigation is needed to fully understand the physics behind the sensors and to design better sensors.

3.4 *Simulations*

To gain a better physical understanding of the change in conductance of the wires when DNA targets and probes are attached, process and device simulations of the

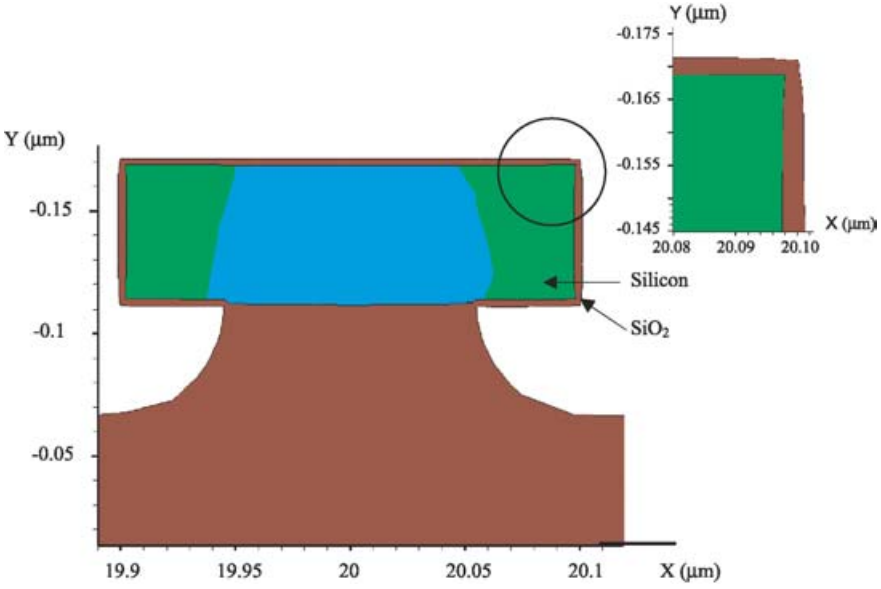

FIGURE 7 Simulated cross section of a 200-nm-wide Si wire on oxide, showing the undercut of the oxide caused by the isotropic oxide etch. The *inset* shows the corner effects during the oxide growth

two-dimensional cross sections of the wires were carried out using the ISE semiconductor simulation tools (ISE, Zurich, Switzerland). The process-modeling module of the tool was used to simulate all the important process steps, capturing the undercut during the isotropic oxide etch, as well as the stress and corner effects during oxide growth at high temperatures, as shown in Fig. 7. The initial doping density within the wire was matched to the values obtained from Hall measurements on implanted planar samples. The software does not model the surface damage and roughness due to various etching steps.

The results from the process simulator were used as the input to the device simulator. To extract the conductance of the wires using two-dimensional device simulations, two artificial electrical contacts were defined on this structure. One contact was assumed to cover the thin oxide surrounding the major portion of the structure, and the second was assumed to be a small point at the center of the wire where the semiconductor is expected to be neutral until the wire is almost fully depleted by surface charges or external electric fields. A schematic of the mesh, along with the contacts, is shown in Fig. 8.

With this choice of electrodes to define the potential around the structure, we solved Poisson's equation throughout the wire cross section to obtain the carrier density and mobility at all points within the wire. Doping- and field-dependent mobility models and Shockley–Read–Hall (SRH) doping-dependent recombination models were used in the simulations [17, 18]. The carrier distribution was assumed to obey Fermi–Dirac statistics, and no quantum effects were included in the simulations.

The only unknown in the physical characteristics of the structure was the magnitude of the fixed charge density at the oxide–semiconductor interface surrounding the wire. We assumed that this charge density remains constant all around the wire; i.e. it is independent of the orientation of the crystal lattice with respect to the oxide interface and also does not depend on possible process-induced damage on selected Si surfaces. The carrier concentration and mobility values were

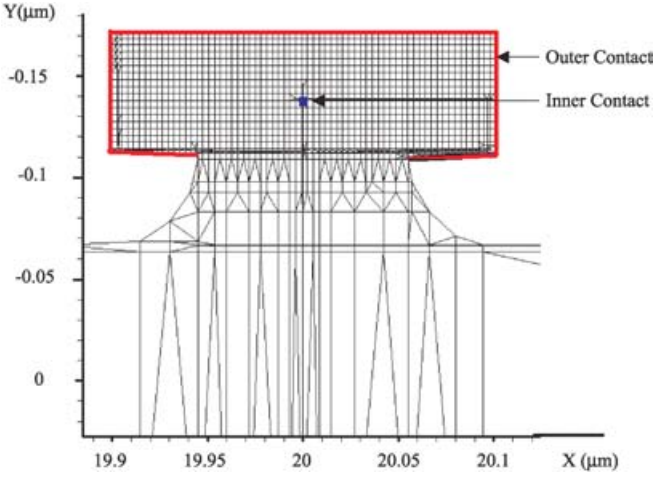

FIGURE 8 Electrical mesh and contacts of the simulated structure; shown for a 200-nm-wide wire

obtained at all points within the wire assuming a constant fixed charge density and zero potential difference between the two artificial electrodes. A good match between the experimentally observed current density of the 200-nm-wide wire and that calculated from the simulation was obtained with a fixed charge density of about 1×10^{12} /cm^2, which is a reasonable number. We then assumed that the fixed charge density remains constant at this value irrespective of the width of the wire, and the conductance values were evaluated as a function of the wire width. A comparison of the calculated values of conductance to the experimental measurements as a function of wire width is plotted in Fig. 3. We observe an excellent agreement between the observed and calculated values of conductance for all except the narrowest width. To provide physical insight into the behavior within the nanowires, the carrier-concentration contours within the wire for two different wire widths – 200 nm and 50 nm – were calculated and are shown in Fig. 9a and b, respectively. These plots of the carrier concentrations clearly show the effect of carrier depletion from the sides of the wire as well as the top. The difference

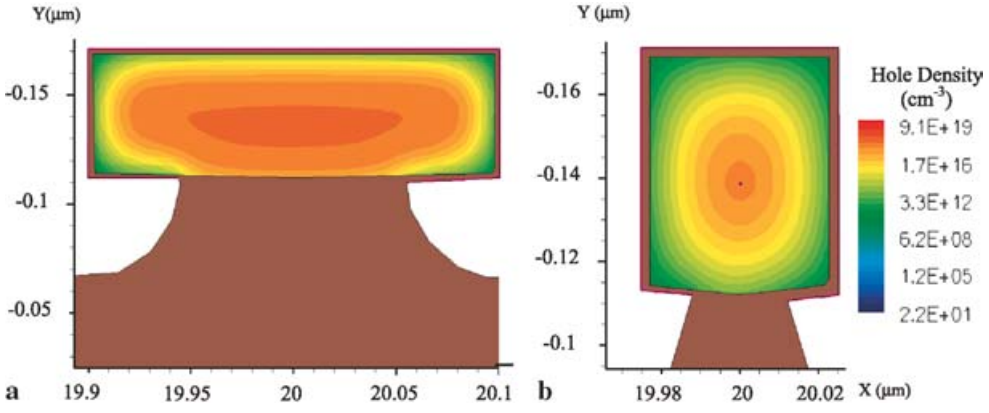

FIGURE 9 Carrier-concentration contours for the 200-nm-wide (**a**) and 50-nm-wide (**b**) wires, assuming a fixed charge density of 1×10^{12} /cm^2 and inner and outer electrodes set to the same potential

shown in Fig. 3 between experimental and simulated values for the 50-nm-wide wire is thus attributed to the significant depletion of carriers within the wire, making the simulation very sensitive to the parameters chosen and the assumption of neutrality at the inner electrode. The experimental data for this wire width also varies significantly from one device to another, again consistent with sensitivity to minor parameter variations.

To evaluate qualitatively the effect of the change in conductance by surface charge from the molecular species, we calculated the dependence of conductance on the surface potential (i.e. the potential difference between the surface of the semiconductor and the bulk of the semiconductor) for two different wire dimensions – 200 nm and 50 nm. This conductance variation is shown in Fig. 10. We observe that the sensitivity of the conductance to changes in surface potential is significantly larger for smaller wires. For a 500 meV change in surface potential, the conductance change for a 50-nm-wide wire is 20 times as great as the change for a 200-nm-wide wire. This again can be explained by the greater efficiency of the surface potential in laterally modulating the carriers for a smaller wire compared to a wider wire, where the dominant modulation is from the top surface. These simulations suggest that the dimensions of the nanowire and the dopant concentration within the nanowire can be adjusted to maximize the sensitivity of the nanowire sensor. The practical limit on the improvement will probably be determined by sensitivity to process variations.

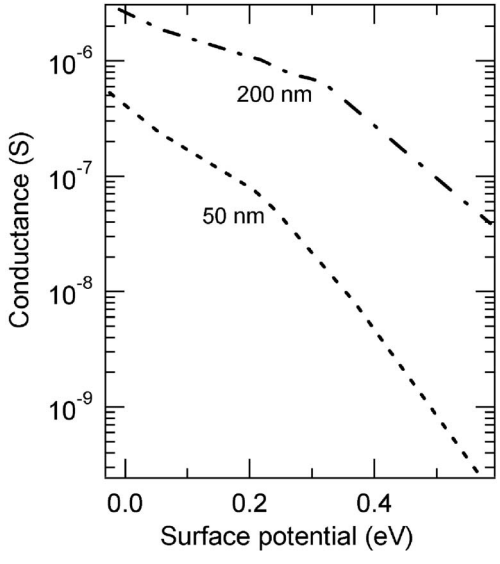

FIGURE 10 Simulated conductance values as a function of the surface potential for the 200-nm-wide and 50-nm-wide wires

4 Conclusions

Highly sensitive and sequence-specific DNA sensors were demonstrated on silicon nanowires (SiNWs) with single-stranded (ss) PNA probes covalently immobilized on their surfaces. The sensitivity of the nanowire sensors depended strongly on the width of the wires. A linear relationship between the response of the sensor and the surface-to-volume ratio was observed for nanowire widths between 800 nm and 100 nm, whereas a nonlinear enhancement appeared for a small wire width of 50 nm. This improved sensitivity corresponded to the nonlinear decrease in the conductance observed for these narrow nanowires. Two-dimensional simulations of the devices suggested that the observed nonlinear decrease in conductance for small wire dimensions can be attributed to the depletion of carriers from all sides by the fixed charges present at the oxide–semiconductor boundary. The fraction of the area depleted of carriers near the vertical sides of the wire is considerably larger for smaller widths than for wider wires. This makes narrower wires more sensitive to changes in surface potential. Thus, we conclude that tuning the two-dimensional carrier depletion can be used to optimize the sensitivity of nanowires.

In addition, compared to label-dependent DNA detecting methods, where fluorescent, chemiluminescent, redox, or radioactive labels are required for signal readout, the label-free DNA detecting method illustrated here offers the advantages of eliminating expensive labeling steps and simplifying the signal readout. Furthermore, the nanoscale features of silicon wires fabricated by 'top-down' semiconductor processing enable fabrication of sensor arrays with extremely high density and capable of being directly integrated with silicon-based circuits.

ACKNOWLEDGEMENTS We would like to thank H. Gamino and M. Flores for assistance with the sample processing, C. Nauka for SPV measurements, and W.F. Stickle, D.K. Bilich, and M. Mellard for XPS and TOF-SIMS characterization. We also thank T.K. Cooney and C.D. Huang for assistance with the simulation tools. This work is partially supported by DARPA.

REFERENCES

1 Y. Xia, P. Yang, Y. Sun, Y. Wu, B. Mayers, B. Gates, Y. Yin, F. Kim, H. Yan: Adv. Mater. **15**, 353 (2003)
2 J. Kong, N.R. Franklin, C. Zhou, M.G. Chapline, S. Peng, K. Cho, H. Dai: Science **287**, 622 (2000)
3 K. Besteman, J. Lee, F. Wiertz, H. Heering, C. Deeker: Nano Lett. **3**, 727 (2003)
4 J. Li, Y. Lu, Q. Ye, M. Cinke, J. Han, M. Meyyappan: Nano Lett. **3**, 929 (2003)
5 Y. Cui, Q.Q. Wei, H.K. Park, C.M. Lieber: Science **293**, 1289 (2001)
6 Z. Li, Y. Chen, X. Li, T.I. Kamins, K. Nauka, R.S. Williams: Nano Lett. **4**, 245 (2004)
7 J. Hahm, C.M. Lieber: Nano Lett. **4**, 51 (2004)
8 M. Law, H. Kind, F. Kim, B. Messer, P. Yang: Angew. Chem. Int. Ed. **41**, 2405 (2002)
9 C. Li, D.H. Zhang, X.L. Liu, S. Han, T. Tang, J. Han, C.W. Zhou: Appl. Phys. Lett. **82**, 1613 (2003)
10 L.A. Chrisey, G.U. Lee, E. O'Ferrall: Nucleic Acids Res. **24**, 3031 (1996)
11 F.N. Rehman, M. Audeh, E.S. Abrams, P.W. Hammond, M. Kenney, T.C. Boles: Nucleic Acids Res. **27**, 649 (1999)
12 M. Beier, J.D. Hoheisel: Nucleic Acids Res. **27**, 1970 (1999)
13 M.C. Homs: Anal. Lett. **35**, 1875 (2002)
14 E. Pavlovic, A.P. Quist, U. Gelius, S. Oscarsson: J. Colloid Interface Sci. **254**, 200 (2002)
15 K. Nauka, T.I. Kamins: J. Electrochem. Soc. **146**, 292 (1999)
16 J. Wang, D. Palecek, P. Nielsen, G. Rivas, X. Cai, H. Shiraishi, N. Dontha, D. Luo, P.A.M. Farias: J. Am. Chem. Soc. **118**, 7667 (1996)
17 J.G. Fossum, D.S. Lee: Solid State Electron. **25**, 741 (1982)
18 G. Masetti, M. Severi, S. Solmi: IEEE Trans. Electron Devices **30**, 764 (1983)